TECHNICAL PAPER

Application of an artificial neural network model to predict the ultimate tensile strength of friction-welded titanium tubes

R. Palanivel[1] · I. Dinaharan[1] · R. F. Laubscher[1]

Abstract

This paper presents an investigation to establish the link between friction welding process parameters and the ultimate tensile strength (UTS) of friction-welded titanium joints by application of an artificial neural network (ANN) technique. The experimental matrix is based on a central composite design with parameters varied at five levels. The UTS of the joints was modeled by the application of the response surface method (RSM). The joint UTS was also simulated by the application of a feed-forward back-propagation ANN with a single hidden layer composing of 20 neurons. The ANN was tested against and trained with the experimental data. The influence of the various parameters on the UTS was assessed by performing a sensitivity analysis. Lastly, the predictions of both the RSM model and the ANN were compared with one another. The results indicate that ANN is indeed a feasible technique for modeling and predicting the effect of process parameters on the UTS for friction welding of titanium tubes. When compared to RSM, ANN displayed a closer agreement with the data. In both cases, however, prediction errors were within 5%. Moreover, the link between the various process parameters and the UTS of the weld joints was also examined and commented upon.

Keywords Titanium · Tube · Friction welding · Ultimate tensile strength · Artificial neural network

1 Introduction

Titanium and its alloys are eminently suitable for use in various industries because of their high corrosion resistance coupled to other mechanical and metallurgical properties such as high specific strength and creep resistance. These include power plant and other selected chemical industries, deep-sea water exploration structures, etc [1–3]. As commercially pure titanium grade 2 has more corrosion resistance, the power plant especially nuclear power plant industry requires effective and efficient joining of titanium grade 2 pipes and/or tubes for fluid transport. A significant problem during welding of titanium is porosity. It is a persistent problem and mostly caused by gas bubbles formed during solidification of weld metal [4]. At present, friction welding is a solid-state joining process used extensively to avoid such melting-related defects. Friction welding has the ability to join certain materials that may otherwise present a challenge when joining by conventional fusion welding techniques [5, 6]. The most significant independent process parameters associated with friction welding are rotational speed, friction time and burn-off length [7–10]. Friction-welded metallic tubes of acceptable standard have been reported by various researchers [11–18]. Shin et al. [11] joined dissimilar zirconium-based bulk metallic glass tubes and recorded the temperature distribution during welding. They carried out microstructural characterization and X-ray diffraction analysis on the weld cross section. Kumar and Balasubramanian [15] joined SUS304HCu austenitic stainless steel tubes. They identified various regions within the joint and reported the microstructure. The welded zone exhibited higher hardness compared to the base material.

The resultant mechanical and metallurgical properties obtained after welding usually define weld quality. More

✉ R. Palanivel
  rpalanivelme@gmail.com

  I. Dinaharan
  dinaweld2009@gmail.com

  R. F. Laubscher
  rflaubscher@uj.ac.za

1 Department of Mechanical Engineering Science, University of Johannesburg, Auckland Park Kingsway Campus, Johannesburg 2006, South Africa

focus is, however, required on techniques for "intelligent" selection of the associated process parameters to attain a predetermined weld quality. Significant time and effort savings may be realized by avoiding trial and error. Numerical modeling-based prediction schemes may therefore fulfill this prediction role for obtaining the best combination of process parameters to obtain the required weld quality. Artificial neural network (ANN)-based modeling is typically more complex than other empirical modeling approaches. It does also require considerable knowledge and experience to apply effectively and has been has been applied mostly for investigating the link between input and output parameters of materials processing techniques [19].

An ANN "learns" from samples and identifies the association between input and output values from a selected sequence of data. It does so without prior expectations as regards the link. It may therefore have the capability for predicting the ultimate tensile strength (UTS) of the welded joints by combining different process parameters without assimilation of any physical evidence about the process standard in its model. ANN modeling has the added advantage that it can keep track of process changes by storing important data that can be altered depending on new data as it becomes available [19–21].

Pal et al. [19] established a multilayered ANN model for prediction of the UTS of pulsed metal inert gas-welded plates and compared the results with a multiple regression analysis. They showed that the ANN model produced better results than the multiple regression analysis. Nagesh and Datta [20] used a back-propagation ANN model to predict the bead geometry and weld penetration and eventually concluded that a 6-10-9-4 network was the optimal network structure. Kim et al. [21] used error back-propagation algorithm and Levenberg–Marquardt approximation algorithm to establish a multilayered ANN for predicting the bead width. Dehabadi et al. [22] used a feed-forward back-propagation ANN to predict the microhardness of friction stir-welded AA6061. They reported that it is possible to save time, material and cost using ANN technique. Nagesh et al. [23] predicted the bead geometry during TIG welding of pure aluminum by ANN. They used a two-level fractional factorial design to conduct conventional experimental work and developed linear regression equations to optimize the process parameters with a genetic algorithm and ANN approach.

Anand et al. [24] compared the response surface method (RSM) with ANN and inferred that ANN solutions are closer to the experimental data when compared to RSM. Acherjee et al. [25] studied the applicability of ANN use for assessing the lap shear strength and weld seam width of laser welding of thermoplastic sheets. Kalidas et al. [26] used ANN and RSM techniques to develop a model for predicting surface roughness of AISI 304 steel for end milling and concluded that satisfactory results can be estimated that fundamentally

diminishes the associated cost and time. Haghdadi et al. [27] simulated the hot deformation flow behavior of an A356 aluminum alloy with the help of a feed-forward back-propagation ANN and concluded that the ANN model is a robust prediction tool. Shojaeefard et al. [28] used an ANN to predict the UTS and hardness of friction stir-welded dissimilar aluminum alloys. Canakci et al. [29] used an ANN technique to predict the volume loss, specific wear rate and surface roughness of metal matrix composites (AA2014/B_4C) and concluded that ANN is the best tool for prediction with minimum cost and time. Sha and Edwards [30] presented details of the most significant difficulties often associated with the use of ANN and subsequently suggested appropriate guidelines for effective use of ANN. Minimization of the error between actual and predicted outputs can be done achieved by continuously adjusting the weights linking the neurons between adjacent layers. Lakshminarayanan and Balasubramanian [31] used design of experimental techniques to develop an RSM and an ANN model, with a back-propagation algorithm, to predict the UTS of friction stir welding of AA7039. The ANN models displayed superior prediction ability when compared to the RSM models.

The literature survey concludes that metallic tubes have been successfully joined by friction welding, but that no such evidence exists for titanium tubes. Joining of grade 2 titanium tubes is required to meet the demands of power plant industries due to its excellent corrosion resistance. Hence, the current investigation is to join grade 2 titanium tubes by friction welding and to establish the feasibility of using an appropriate ANN model to predict the UTS of the joints. Input parameters for the networks are rotational speed, friction time and burn-off length, whereas the measured output is UTS. Statistical analysis is performed for assessing the suitability of the proposed model.

2 Experimental procedure

2.1 Development of design matrix

Design of experiments techniques allows "intelligent" experimental design to investigate the effect of various process parameters in a practical manner with the minimum number of experimental trials (runs). Hence, significant time and resources can be saved. According to a literature review, the most significant process parameters associated with friction welding are rotational speed (N), friction time (T) and burn-off length (D). For the current investigation, a three-parameter five-level central composite design (CCD) consisting of 20 trials of coded conditions including of a full factorial $2^3 = 8$ is utilized. The parameters at the transitional (0) level establish the six center points, whereas the grouping of each process parameter at its lowermost or uppermost ranges with

the other six parameters of the transitional levels establishes the star points. This implies 20 investigational runs to evaluate possible linear, quadratic and other two-way interaction effects of the process parameters on the response. The coded values of the maximum and minimum ranges of the process parameters were $+1.682$ and -1.682, respectively. The intermediate values were obtained as follows:

$$X_i = 1.682 \left[2X - (X_{\max} + X_{\min}) \right] / \left[(X_{\max} - X_{\min}) \right] \quad (1)$$

where X_i is the required coded value of a variable X; X is any value of the variable from $X_{\min}$ to $X_{\max}$; $X_{\min}$ is the minimum level of the variable; and $X_{\max}$ is the maximum level of the variable. The process parameter ranges as used were selected based on selected trial experiments and relevant literature. The process parameter limits were chosen based on the weld bead displaying a symmetric appearance without major defects. This was confirmed by visual inspection. The maximum, minimum and intermediate values of the selected parameters are presented in Table 1. The design matrix for friction welding of the tubes is presented in Table 2. Secondary process parameters such as the forging force (30 kN), friction force (20 kN) and forging time (22 s) were kept constant for all experiments.

2.2 Welding of titanium tubes

The workpiece material is commercially pure grade 2 titanium tube with outer diameter of 60 mm, length of 75 mm and wall thickness of 3.9 mm. A friction welding machine developed by M/s Profile Tooling at Nelson Mandela Metropolitan University, South Africa, was used to carry out welding. Misalignment between the tubes during setup and rotation was controlled by clamping the tubes in a specially designed fixture (see Fig. 1). Shielding was provided by supplying Argon gas to the weld area in order to avoid oxidation of the titanium. The faying surface of the tubes was cleaned with acetone prior to welding. Figure 2 displays a batch of the friction-welded tubes. A water jet cutting machine was used to extract tensile specimen with a 40 mm gauge length and width of 6 mm. Figure 3 shows the extracted tensile specimen. Mechanical properties including UTS were obtained by computerized tensile testing. The UTS values as obtained experimentally from each combination of process parameters are given in Table 3. Metallurgical studies were

Table 2 Friction welding process parameter (inputs)

Trial run	Friction welding process parameter		
	Design matrix coded value		
	N	T	D
1	-1	-1	-1
2	-1	-1	1
3	-1	1	-1
4	-1	1	1
5	1	-1	-1
6	1	-1	1
7	1	1	-1
8	1	1	1
9	-1.682	0	0
10	1.682	0	0
11	0	-1.682	0
12	0	1.682	0
13	0	0	-1.682
14	0	0	1.682
15	0	0	0
16	0	0	0
17	0	0	0
18	0	0	0
19	0	0	0
20	0	0	0

also carried out to see the macro- and microstructure of the welded joints.

2.3 Development of response surface methodology (RSM) models

The UTS of friction-welded joints is a function of rotational speed (N), friction time (T) and burn-off length (D) which is expressed as:

$$\text{UTS} = f(N, T, D) \quad (2)$$

where N is the rotational speed, rpm, T the friction time, s, and D the burn-off length, mm.

For three parameters, the chosen polynomial is expressed as follows:

$$\text{UTS} = b_0 + b_1 N + b_2 T + b_3 D + b_{11} N^2 + b_{22} T^2 \\ + b_{33} D^2 + b_{12} NT + b_{13} ND + b_{23} TD \quad (3)$$

Table 1 Friction welding parameters and their levels

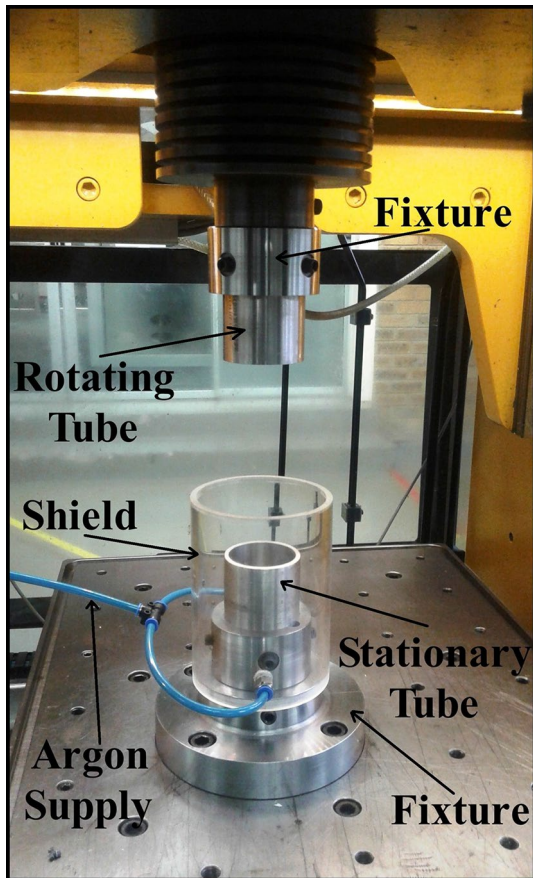| No.	Parameter	Notation	Unit	Levels				
				-1.682	-1	0	1	1.682
1	Rotational speed	N	rpm	1695	1900	2200	2500	2705
2	Friction time	T	s	25	28	32	36	39
3	Burn-off length	D	mm	0.7	1.0	1.4	1.8	2.1

Fig. 1 Fixture designed for friction welding of tubes

Fig. 2 Friction-welded tubes

Fig. 3 Sample tensile specimens extracted from the tubes

where b_0 is the average of responses and b_1, b_2, b_3, b_2, b_{11}, b_{22}, b_{33}, b_{12}, b_{13} and b_{23} are the response coefficients that depend on respective main and secondary interaction effects of parameters.

The response coefficients were calculated using SYSTAT 12 statistical software. The RSM model obtained from the analysis is presented as follows:

$$UTS(MPa) = 313.697 + 7.342N - 6.989T + 6.247D$$
$$- 23.791N^2 - 19.903T^2 - 16.192D^2 - 0.5TN + 2ND + TD \quad (4)$$

The suitability of the model was evaluated by an analysis of variance (ANOVA) and is presented in Table 4. The calculated F ratio was higher than that of the tabulated values at the 95% confidence level; hence, the model was deemed adequate. The goodness of fit of the model was also evaluated by calculating the coefficient of determination (R^2). Typically, a R^2 value in excess of 0.8 may be considered as an adequate representation of the underlying process. R^2 values of 0.96 were obtained for the current model. This implies that 96% of the variance in the experimental details is predictable from the variation in the process parameters. The value of the adjusted R^2 of 0.93 is also sufficiently high for the confidence in the model.

2.4 Artificial neural network modeling

An ANN typically refers to a computational model that is developed based on the characteristics of a biological network. The structure of the model typically encompasses combinations of computational units referred to as neurons, cells, nodes or units. In an ANN model, neurons are interrelated with each other with the help of unidirectional or bidirectional communication links, each of which is allocated a weight. The weights represent information being used by the network to solve a problem [24–27]. Normalization of the input variables is conducted for a faster approach toward the global minima and increased accuracy of the network. The following equation is applied to normalize the input and output of the experimental values between the range of 0.1 to 0.9 [28]:

$$Y_i = 0.1 + 0.8(Z_i - Z_{min})/(Z_{max} - Z_{min}) \quad (5)$$

where Y_i is the normalized input/output value, Z_i the actual input/output value, Z_{max} the maximum input/output value and Z_{min} the minimum input/output value.

An ANN system consists typically of a three-layered system, i.e., input layer, an output layer and hidden layers associated with the neuron processing units. Figure 4 presents an example of a feed-forward back-propagation system with a three-layered structure. The input layer contains three nodes, which represent the rotational speed, friction time and burn-off length. The UTS is represented with only one

Table 3 Responses of the friction welding process parameters (output)

Trail run	Ultimate tensile strength					% error $\frac{E-P}{E} \times 100$	
	Experimental value (E), MPa		Prediction value (P), MPa				
	Actual	Normalized	Normalized	Actual	RSM	ANN	RSM
1	250	0.236	0.216	247.81	248.99	0.884	0.405
2	263	0.355	0.350	262.50	255.47	0.192	2.947
3	235	0.100	0.100	235.02	234.01	−0.010	0.421
4	239	0.136	0.140	239.40	244.49	−0.168	−2.247
5	271	0.427	0.430	271.30	260.67	−0.110	3.962
6	279	0.500	0.500	279.38	275.15	−0.136	1.398
7	241	0.155	0.175	243.21	243.69	−0.907	−1.105
8	266	0.382	0.380	265.80	262.17	0.076	1.459
9	235	0.100	0.100	235.00	234.04	0.255	0.409
10	253	0.264	0.260	252.60	258.74	0.159	−2.217
11	259	0.318	0.320	259.20	269.14	−0.077	−3.769
12	251	0.245	0.256	252.14	245.63	−0.453	2.185
13	255	0.282	0.280	254.79	255.33	0.082	−0.130
14	276	0.473	0.582	288.03	276.32	−4.178	−0.117
15	315	0.827	0.829	315.19	313.70	−0.061	0.415
16	323	0.900	0.829	315.19	313.70	2.477	2.966
17	309	0.773	0.829	315.19	313.70	−1.964	−1.497
18	305	0.736	0.829	315.19	313.70	−3.233	−2.772
19	319	0.864	0.829	315.19	313.70	1.208	1.690
20	312	0.800	0.829	315.19	313.70	−1.012	−0.541

Table 4 ANOVA results of the developed RSM models

Response	Source	Sum of squares	Degrees of freedom	Mean square	F-ratio (calculated)	F-ratio (tabulated)
UTS	Regression	16,817.035	9	1868.559	31.031	2.92
	Residual	602.165	10	60.216		
R^2	0.965					
Adjusted R^2	0.934					
SE	7.760					

Fig. 4 Neural network architecture
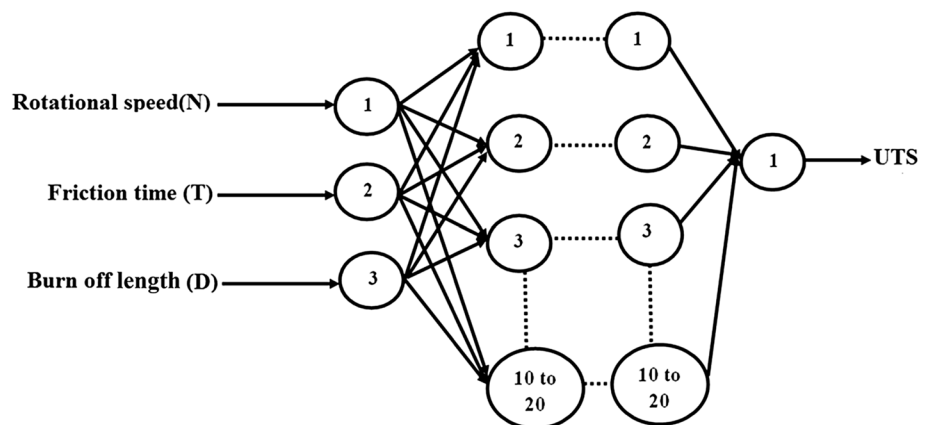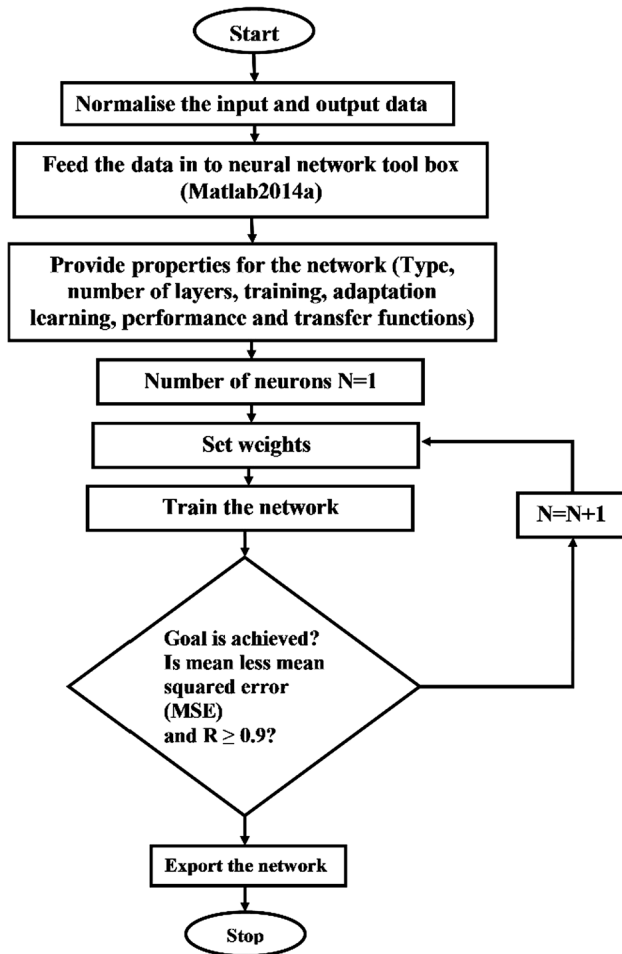
Fig. 5 Flowchart of artificial neural network development using neural network tool

node making up the output layer. The architecture (number of neurons and layers used) of the hidden layer is based on an assessment of a number of training samples. The ANN eventually used has three input neurons associated with the three process parameters and one hidden layer containing 10 to 20 neurons each. The ontogeny (origin and development) of the ANN is presented in Fig. 5.

There is no specific rule allocation of data for training, testing and validation. However, the common rule is that the training data should be more than testing and validation [26]. Hence, 70% of data were used for training, 15% of data were used for testing and remaining 15% of data were used for validation. Thus, in total, 14 data points were used for training, 3 for testing and 3 for validation.

The network was trained using a Levenberg–Marquardt algorithm. MATLAB version R2014a software was used to train the network numerous times by considering 1000 epochs to achieve an acceptable performance [24]. In this study, the network was trained for 780 epochs. While training the network, weights and biases are iteratively adjusted to minimize the performance function mean squared error

[30]. The active function has been chosen as the typical values of MATLAB function "trainlm." Mean squared error was considered to evaluate the performance of the network [26]. Mean squared error should be a minimum for the entire experimental data set. The optimum validation performance achieved for a mean squared error of 0.000309 was attained at 774 epochs (depicted in Fig. 6). This low value indicates good prediction accuracy. These simulated results were then further assessed and used with MATLAB.

Table 3 presents UTS values predicted by the ANN. The accuracy of the ANN predictions was assessed by performing a regression analysis to calculate a correlation coefficient [24]. Best-fit curves were also developed for training, testing and validation of the ANN used. Figure 7 provides an indication of the accuracy of the ANN estimation by comparing curves of best fit for training, testing, validation and UTS against experimental data. Correlation coefficients of 0.989, 1, 1 and 0.989 were obtained for the training, testing, validation and UTS. This implies a very close correlation between the ANN model and the experimental data. The ability of the ANN, as developed and used, to predict the effect of the various input parameters on the UTS is assessed by calculating a mean prediction error (%) [25]:

Mean prediction error (%)

$$= 1/P \sum_{1}^{P} \frac{|\text{Experimental value} - \text{Predicted value}|}{\text{Experimetnal value}}$$

$$\times 100$$

2.5 Sensitivity analysis

A sensitivity analysis was performed to recognize the most significant parameters along with their predispositions for model validation where the intention is to compare the predicted outputs to the experimental results. The order of importance of the various parameters can then also be established. A
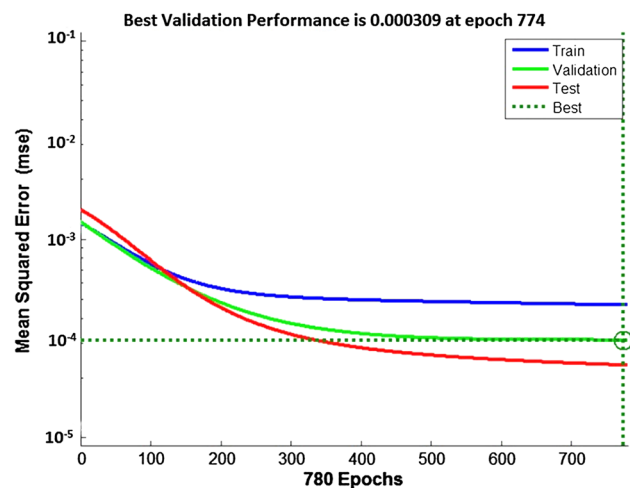
Fig. 6 Network training to predict UTS

Fig. 7 Line of best fit and correlation coefficient between actual and predicted values for training, validation, testing and all UTS data
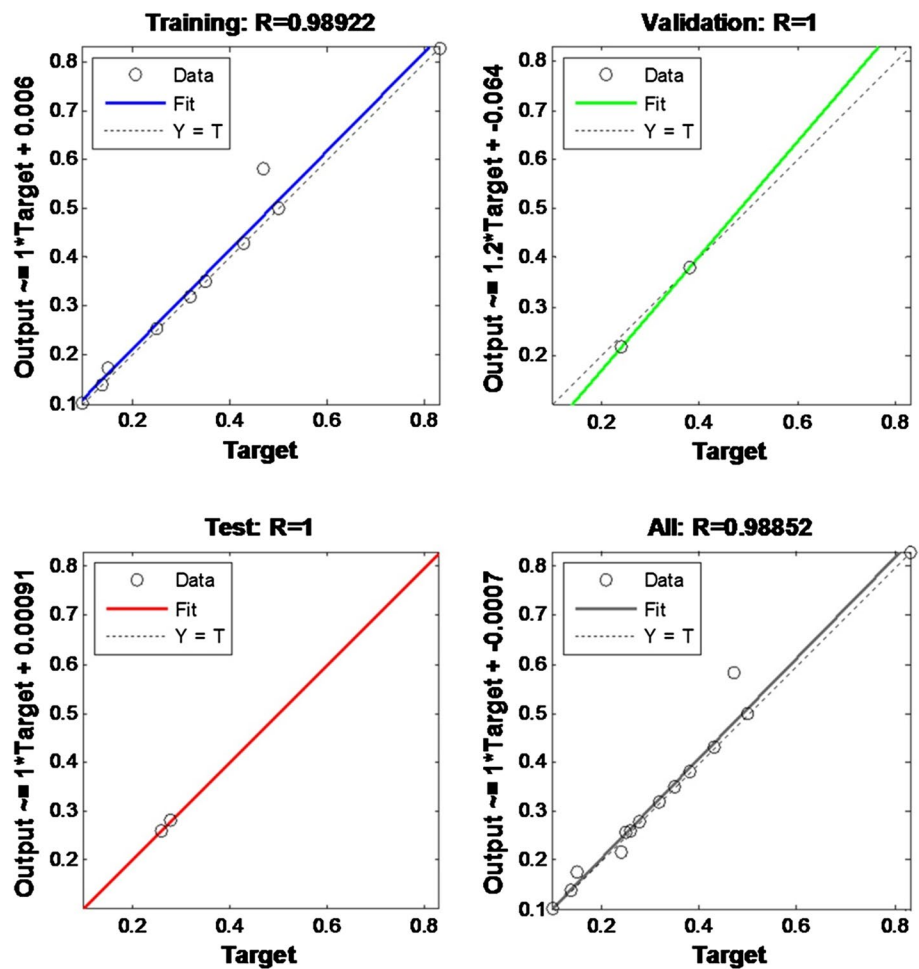
sensitivity analysis provides evidence about the influence of an individual parameter toward its effect on the design objectives. To assess the impact of an input parameter on the output, a training data sensitivity analysis is carried out.

The mathematical sensitivity equation is the partial derivative of the function with respect to its variables [31]. The sensitivity Eqs. (6), (7) and (8) represent the sensitivity of UTS as a function of rotational speed, friction time and burn-off length, respectively.

$$\frac{\partial(\text{UTS})}{\partial N} = 7.342 - 47.582N - 0.5T + 2D \tag{6}$$

$$\frac{\partial(\text{UTS})}{\partial T} = -6.989 - 39.806T - 0.5N + 1D \tag{7}$$

$$\frac{\partial(\text{UTS})}{\partial D} = 6.247 - 32.384D + 2N + 1T \tag{8}$$

Essentially the intention of this work is to be able to predict the variation of the UTS as a function of a small change in the appropriate process parameter. Increasing sensitivity values suggest an increase in the objective function for a minor variation in the design parameter, while decreasing values suggest the opposite [31]. Figure 8 shows the sensitivity of UTS as a function of rotational speed, friction time and burn-off length, respectively. The rotational speed had significant effect on UTS; hence, it produced both negative and positive values (Fig. 8a) and symmetric trend with respect to mean speed. A small variation in the rotational speed causes large changes in UTS. The results reveal that the UTS is more sensitive to rotational speed than friction time and burn-off length.

2.6 Comparison

The importance of any response parameter is relatively easy to assess with RSM models by comparing the appropriate coefficients of the regression model. Recognizing the most significant or insignificant parameter is easily done by assessing the coefficients for the linear and/or quadratic terms in the model. However, this method requires a suitable range for each parameter to ensure that the response(s) under consideration changes in a consistent manner within this range. ANN models usually require a significant number of
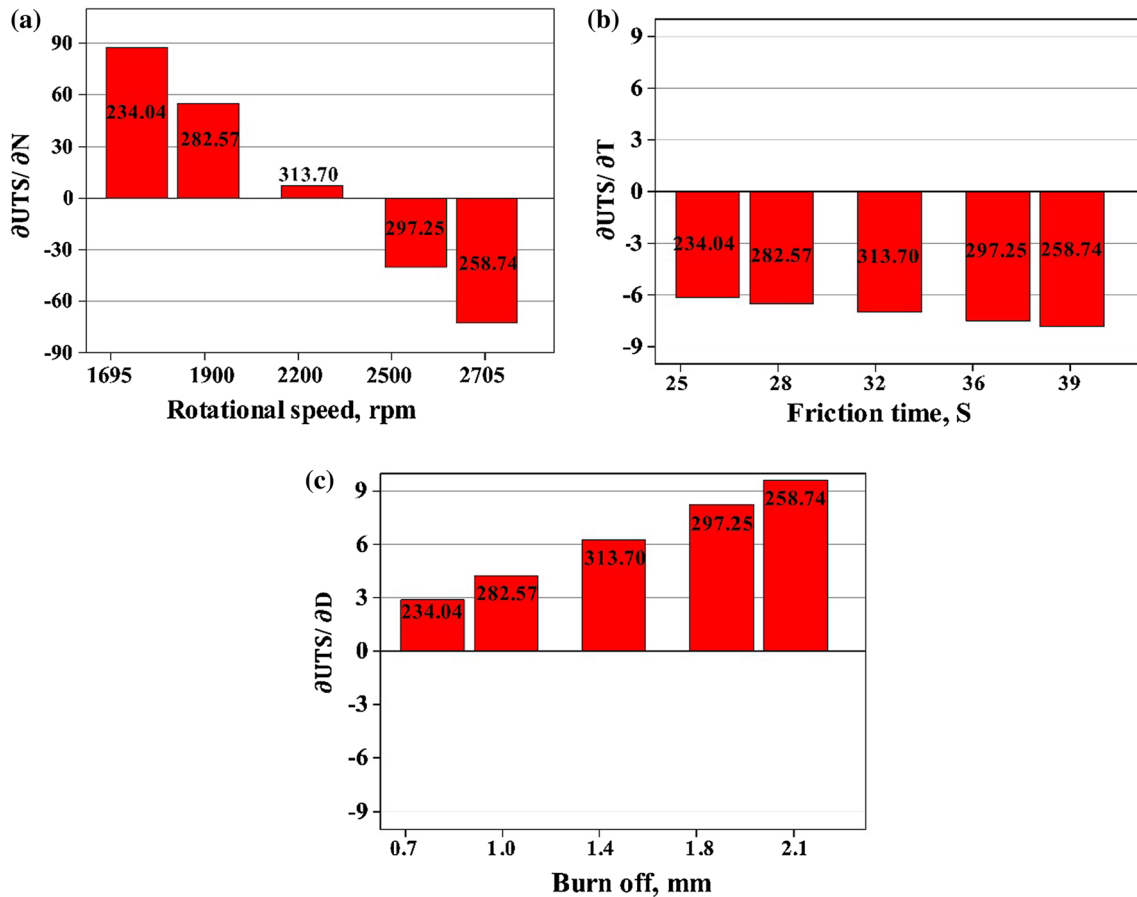
Fig. 8 Sensitivity analysis result: **a** rotational speed (*N*), **b** friction time (*T*), **c** burn-off length (*D*)

repetitive calculations to develop; however, for RSM models one-step calculation is usually enough. The development of ANN models may require significant computational resources based on the problem with nonlinearity and the number of constraints involved. Typically, higher processing cost is required to create an ANN model when compared to RSM. Although the processing cost for ANN models is usually higher than RSM models, ANN models are typically more accurate [31]. Due to the high prediction rate of the ANN model compared to the traditional model, it is useful for rapid prediction of the effect of friction welding process parameters. The comparative performance of the ANN and RSM models in terms of error (%) is presented in Fig. 9. The mean prediction error of the ANN model is 0.707 compared to 1.628 for the RSM model. This implies that the ANN model was marginally more accurate. The actual experimental data for the UTS are compared with the predicted values for ANN and RSM, in Fig. 10. Figures 9 and 10 show that the ANN model displayed increased parity with the experimental results than the RSM model.
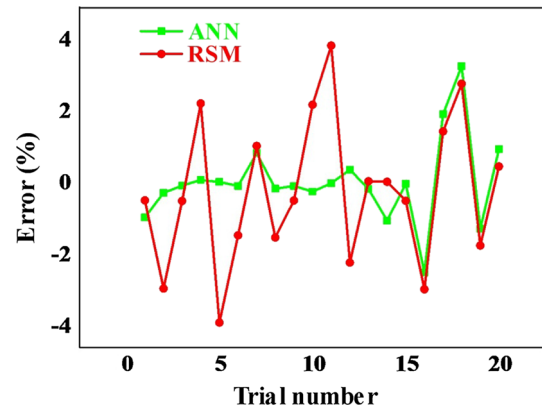
Fig. 9 Comparison of percentage of errors

2.7 Effects of process parameters

Figure 11 shows the microstructure of the base material and transition zone of the welded tube. The effect of rotational speed on the macrostructure, microstructure and failure location is graphically presented in Table 5. It is evident from
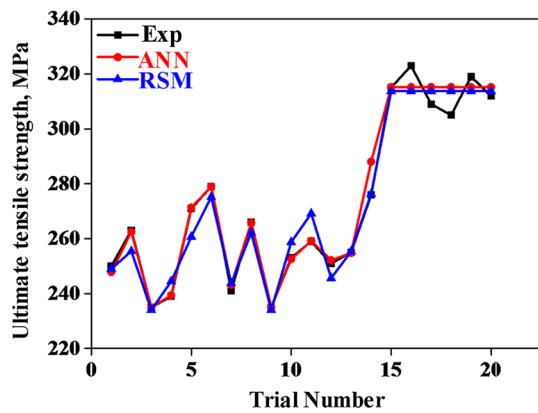
Fig. 10 Comparison plots of UTS

the macrographs (see Table 5) that rotational speed has some effect on the weld zone geometry and flash morphology. The weld zone (WZ) biconcavity and flash size are increased with increasing rotational speed. The width of WZ does, however, decrease with increasing rotational speed. This is due to a more rapid introduction of the frictional heat and subsequent plasticizing during the forging stage. The symmetry of flash between the inner and outer sides is lost with higher rotational speed. More flash is visible on outer side of welded tube due to the increased ejection of material from the interface of weld. The micrographs depicting the structure were taken at the midpoint of the WZ. The average measured grain sizes were 2.5 μm and 1.2 μm at 1600 rpm and 2800 rpm, respectively. Very finer grains were observed by increasing rotational speed. The grain size depends mostly on the frictional heat and deformation rate. However, these two parameters having an opposite effect to each as regards the grain size. The grains may grow and coarsen with an increase in frictional heat at higher rotational speed. On the other hand, grain growth is restricted and an increase in rotational speed assists to fragment the formed grains due to an increased deformation rate. An increase in rotational speed increases the both the heat generation and deformation rates. The smaller grain sizes displayed at the higher
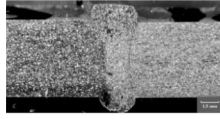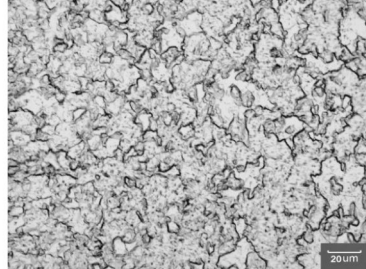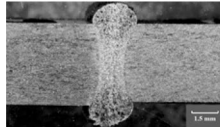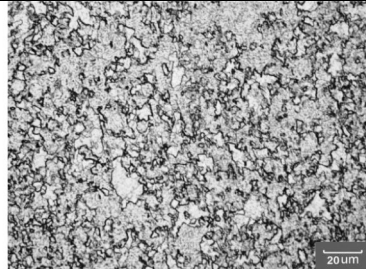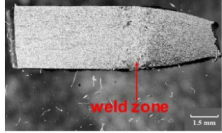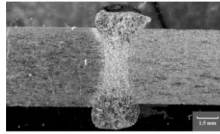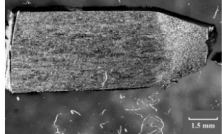
rotational speeds showed that the effect of deformation rate is more dominant. The effect of rotational speed on the UTS is shown in Fig. 12. The UTS increased from 234 MPa at 1695 rpm to a maximum of 314 MPa at 2200 rpm before decreasing to 259 MPa at 2705 rpm. The amount of material that is fully plasticized is low at 1695 rpm which leads to poor consolidation at the forging stage. Tensile failure occurred in the WZ at 1695 rpm (see Table 5). An increase in rotational speed produces more heat and increases the available plasticized material and consequently an improved consolidation during forging. Failure during tensile testing then occurs in the base material (BM) at 2200 rpm, which yields a higher UTS. An increase in rotational speed beyond 2200 rpm leads to excess heat and therefore plasticized material that is expelled at a higher rate from the interface, and failure occurs in the WZ. Hence, the UTS is lower at 2705 rpm.

The effect of friction time on the macro- and microjoint properties is presented in Table 6. The results show that friction time has a significant effect on weld size and flash morphology. Exposure to the frictional heat depends mostly on the friction time. An increased friction time leads to an increased heat production and subsequent joint temperature and conduction. Hence, less flash is observed at the lowest friction time when compared to the higher friction time. The grain size reduced with an increase in friction time. The average grain size reduced from 2.2 to 1.3 μm for an increase in friction time from 25 to 39 s. This is once again the result of the deformation rate dominating the process resulting in increased fragmentation of the grains and grain growth being restricted. The effect of friction time on the UTS is shown in Fig. 13. Once again, a local maximum (314 MPa) for the UTS is displayed at the intermediate fiction time of 32 s with the failure occurring in the base metal. Shorter and longer friction times than the optimum displayed a significant reduction in the UTS. In essence, the reason for this behavior is similar to the effect of rotational speed. Shorter frictional times produce less heat, and the volume of plasticized material is therefore limited leading to reduced consolidation during forging and failure occurs in

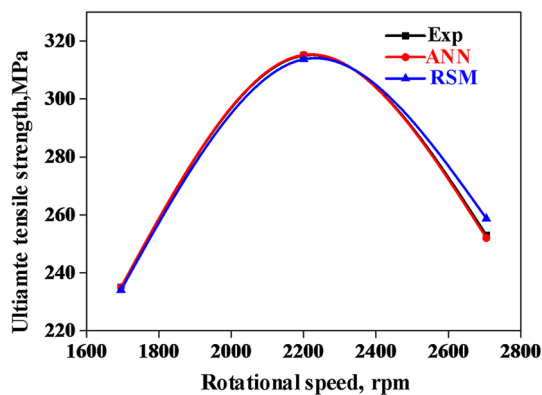**Fig. 11** Microstructure of the base materials and transition zone of the welded tube
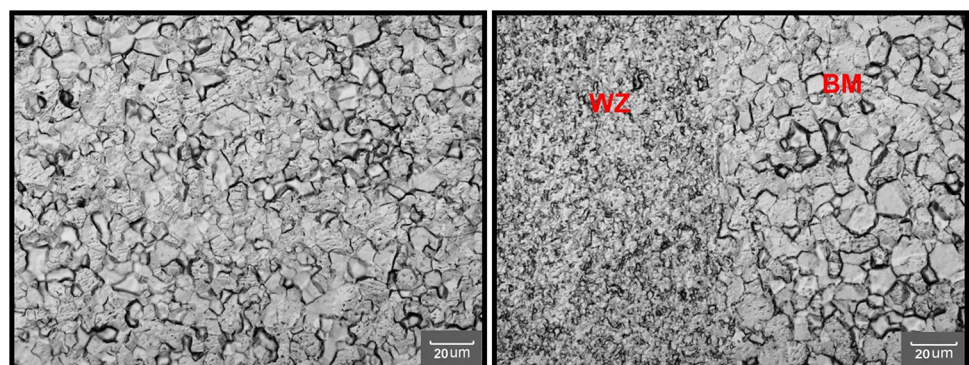
Table 5 Effect of rotational speed on macrostructure, microstructure and failure location of friction-welded tube

Trail No	Macrograph	Microstructure	Failure location
9			
15			
10			

the WZ (see Table 6). Longer friction times produces excess heat and plasticized material that leads to excessive material expulsion from the interface during the forging stage and a less than optimum weld joint with failure during tensile testing also occurring in the weld zone.
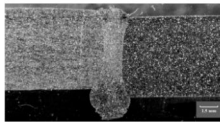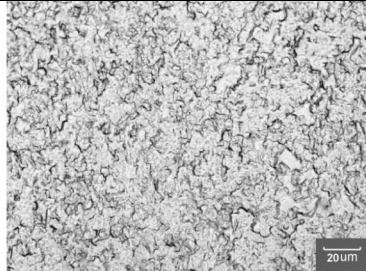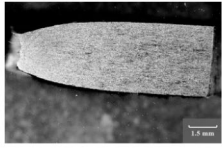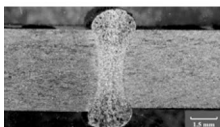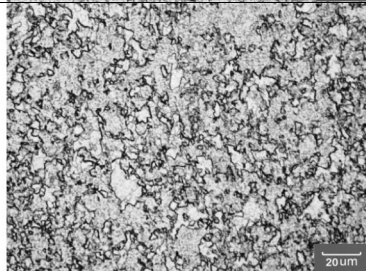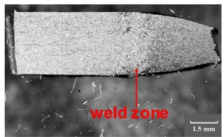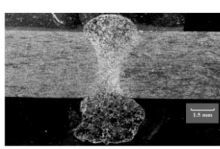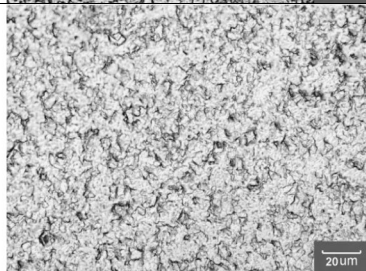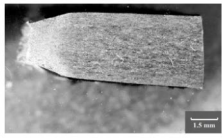
The effect of burn-off length on the macro- and microjoint properties is presented in Table 7. Burn-off length is the length reduction of the tube as a result of the forging stage. Burn-off length can also be considered as an output

Fig. 12 Effect of rotational speed on UTS

parameter [8, 9]. In this study, it is considered as an input because of the process design development in the friction welding machine. It can be observed that the burn-off length influences the size of the weld zone and flash size. Increased flash size and reduced width of the weld zone are observed with an increasing burn-off length. This is due to the ejection of increased volumes of plasticized materials from the joint interface during welding. Different grain sizes were observed for different burn-off lengths and are also presented in Table 7. A relatively small increase in grain size from 1.4 to 1.8 µm was observed for an increase in burn-off length from 0.7 to 2.1 mm. An increased burn-off length does not imply additional frictional heat. Hence, the recrystallized material is produced before forging. An increased burn-off length implies increased material ejection and is the reason for the limited increment in grain size. The effect of burn-off length on the UTS is presented in Fig. 14. The UTS displays a maximum of 314 MPa at 1.4 mm. A shorter or longer burn-off length than the optimum of 1.4 mm leads to a reduction in the UTS with a minimum of 257 MPa at 0.7 mm. An optimum bead expulsion is required to obtain adequate consolidation during forging. Failure during the tensile test therefore occurs in the base metal for the optimum burn-off length (1.4 mm). Failure occurs in the weld zone for the lowest (0.7 mm) and highest (2.1 mm) burn-off
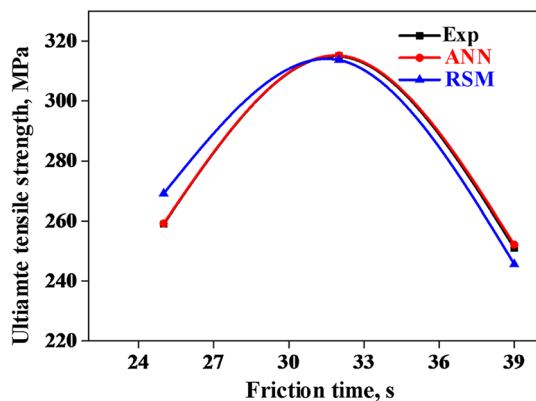
Table 6 Effect of friction time on macrostructure, microstructure and failure location of friction-welded tube

Trail No	Macrograph	Microstructure	Failure location
11			
15			
12			

lengths. If the burn-off length is too low, the expulsion rate will be low, and consequently, the plasticized material is not adequately consolidated during forging. An increase in burn-off length to the optimum distance increases the expulsion of material and optimum consolidation occurs. A further increase in burn-off length expels much of the plasticized and recrystallized material, and the joint approaches a cold weld and experiences a loss in UTS.
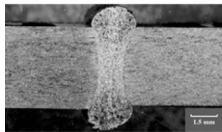

Fig. 13 Effect of friction time on UTS
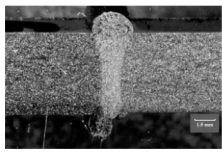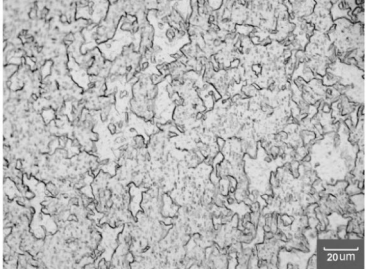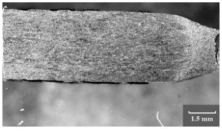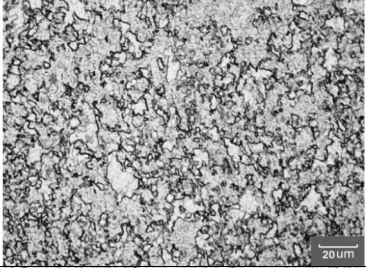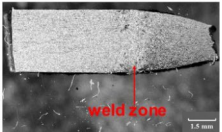
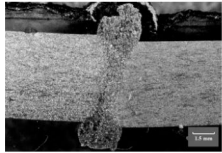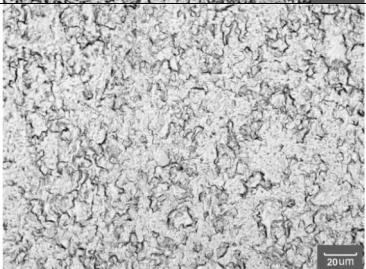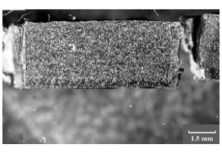## 3 Conclusions

This paper presented RSM and ANN models to predict the UTS of continuous drive friction welding of titanium tubes in terms of its process parameters that include rotational speed, friction time and burn-off length. The viability and performance of the two models were then compared with one another and the experimental results. The results showed that the ANN model is statistically more accurate and is a robust tool to describe and predict the UTS of friction-welded titanium tubes for the process parameters evaluated. Rotational speed and frictional time were identified as the most and least significant process parameters as regards UTS. Both ANN and RSM modelings were shown to be effective tools for modeling of the weld joints obtained during friction welding of commercially pure titanium tubes. ANN produced the most accurate predictions. The variation of rotational speed, friction time and burn-off length has significant effect on the flash size, extent of the WZ, grain size and the failure location when subjected to tensile testing.

Table 7 Effect of burn-off length on macrostructure, microstructure and failure location of friction-welded tube

Trail No	Macrograph	Microstructure	Failure location
13			
15			
14			
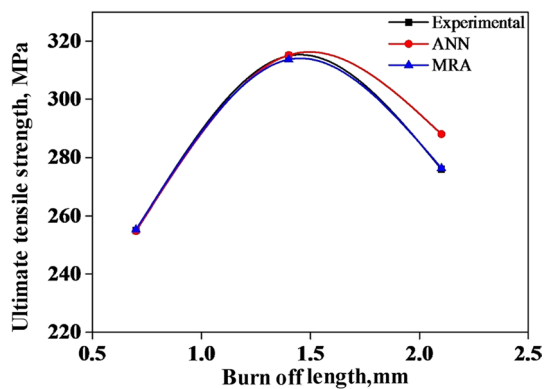
Fig. 14 Effect of burn-off length on UTS

References

1. Ali MH, Ansari MNM, Khidhir BA, Mohamed B, Oshkour AA (2014) Simulation machining of titanium alloy (Ti–6Al–4V) based on the finite element modeling. J Braz Soc Mech Sci Eng 36:315–324
2. Boyer RR (1996) An overview on the use of titanium in the aerospace industry. Mater Sci Eng A 213:103–114
3. Banerjee D, Williams JC (2013) Perspectives on titanium science and technology. Acta Mater 61:844–879
4. Kumar A, Sapp M, Vincelli J, Gupta MC (2010) A study on laser cleaning and pulsed gas tungsten arc welding of Ti–3Al–2.5V alloy tubes. J Mater Process Technol 210:64–71
5. Beloshapkin GV, Beloshapkin MV, Pisarov VK, Stolberov VE, Chernov VA (2007) Friction welding of pipes. Weld Int 21:458–459
6. Prasad KR, Sridhar VG (2016) Evaluating the capability, joining and characterization of similar and dissimilar pipes by friction welding process-review. Int J Appl Eng Res 11:3681–3688
7. Paventhan R, Lakshminarayanan PR, Balasubramanian V (2011) Prediction and optimization of friction welding parameters for joining aluminium alloy and stainless steel. Trans Nonferrous Met Soc China 21:1480–1485
8. Udayakumar T, Raja K, Abhijit AT, Sathiya P (2013) Experimental investigation on mechanical and metallurgical properties of super duplex stainless steel joints using friction welding process. J Manuf Process 15:558–571
9. Selvamani ST, Palanikumar K, Umanath K, Jayaperumal D (2015) Analysis of friction welding parameters on the

mechanical metallurgical and chemical properties of AISI 1035 steel joints. Mater Des 65:652–661

10. Vairamani G, Kumar ST, Malarvizhi S, Balasubramanian V (2013) Application of response surface methodology to maximize tensile strength and minimize interface hardness of friction welded dissimilar joints of austenitic stainless steel and copper alloy. Trans Nonferrous Met Soc China 23:2250–2259

11. Singh J, Gill SS (2008) Multi input single output fuzzy model to predict tensile strength of radial friction welded GI pipes. Int J Inf Syst Sci 4:462–477

12. Faes K, Dhooge A, Baets PD, Donckt EVD, Waele WD (2009) Parameter optimisation for automatic pipeline girth welding using a new friction welding method. Mater Des 30:581–589

13. Shin HS, Parka JS, Yokoyama Y (2010) Dissimilar friction welding of tubular Zr-based bulk metallic glasses. J Alloys Compd 504:S275–S278

14. Kimura M, Ichihara A, Kusaka M, Kaizu K (2012) Joint properties and their improvement of AISI 310S austenitic stainless steel thin walled circular pipe friction welded joint. Mater Des 38:38–46

15. Kumar MV, Balasubramanian V (2014) Microstructure and tensile properties of friction welded SUS 304HCu austenitic stainless steel tubes. Int J Press Vessels Pip 113:25–31

16. Kimura M, Sakaguchi H, Kusaka M, Kaizu K, Takahashi T (2015) Characteristics of friction welding between solid bar of 6061 Al alloy and pipe of Al-Si$_{12}$CuNi Al cast alloy. J Mater Eng Perform 24:4551–4560

17. Rovere CAD, Aquino JM, Ribeiro CR, Silva R, Alcântara NG, Kuri SE (2015) Corrosion behavior of radial friction welded supermartensitic stainless steel pipes. Mater Des 65:318–327

18. Kimura M, Kusaka M, Kaizu K, Nakata K, Nagatsuka K (2016) Friction welding technique and joint properties of thin-walled pipe friction-welded joint between type 6063 aluminum alloy and AISI 304 austenitic stainless steel. Int J Adv Manuf Technol 82:489–499

19. Pal S, Pal SK, Samantaray AK (2008) Artificial neural network modeling of weld joint strength prediction of a pulsed metal inert gas welding process using arc signals. J Mater Process Technol 202:464–474

20. Nagesh DS, Datta GL (2002) Prediction of weld bead geometry and penetration in shielded metal-arc welding using artificial neural networks. J Mater Process Technol 123:303–312

21. Kim IS, Son JS, Lee SH, Yarlagadda PKDV (2004) Optimal design of neural networks for control in robotics arc welding. Rob Comput Integr Manuf 20:57–63

22. Dehabadi VM, Ghorbanpour S, Azimi G (2016) Application of artificial neural network to predict Vickers microhardness of AA6061 friction stir welded sheets. J Cent South Univ 23:2146–2155

23. Nagesh DS, Datta GL (2010) Genetic algorithm for optimization of welding variables for height to width ratio and application of ANN for prediction of bead geometry for TIG welding process. Appl Soft Comput 10:897–907

24. Anand K, Shrivastava R, Tamilmannan K, Sathiya P (2015) A comparative study of artificial neural network and response surface methodology for optimization of friction welding of Incoloy 800 H. Acta Metall Sin (Engl Lett) 28:892–902

25. Acherjee B, Mondal S, Tudu B, Misra D (2011) Application of artificial neural network for predicting weld quality in laser transmission welding of thermoplastics. Appl Soft Comput 11:2548–2555

26. Kalidass S, Palanisamy P (2014) Prediction of surface roughness for AISI 304 steel with solid carbide tools in end milling process using regression and ANN Models. Arab J Sci Eng 39:8065–8075

27. Haghdadi N, Zarei-Hanzaki A, Khalesian AR, Abedi HR (2013) Artificial neural network modeling to predict the hot deformation behavior of an A356 aluminum alloy. Mater Des 49:386–391

28. Shojaeefard MH, Behnagh RA, Akbari M, Givi B, Farhani F (2013) Modeling and Pareto optimization of mechanical properties of friction stir welded AA7075/AA5083 butt joints using neural network and particle swarm algorithm. Mater Des 44:190–198

29. Canakci A, Ozsahin S, Varol T (2014) Prediction of effect of reinforcement size and volume fraction on the abrasive wear behavior of AA2014/B$_4$Cp MMCs using artificial neural network. Arab J Sci Eng 39:6351–6361

30. Sha W, Edwards KL (2007) The use of artificial neural networks in materials science-based research. Mater Des 28:1747–1752

31. Lakshminarayanan AK, Balasubramanian V (2009) Comparison of RSM with ANN in predicting tensile strength of friction stir welded AA7039 aluminium alloy joints. Trans Nonferrous Metals Soc China 19:9–18